



ARTICLE

<https://doi.org/10.1038/s41467-019-10694-z>

OPEN

Mechanisms of Ca^{2+} /calmodulin-dependent kinase II activation in single dendritic spines

Jui-Yun Chang^{1,2}, Yoshihisa Nakahata², Yuki Hayano ² & Ryohei Yasuda ²

CaMKII α plays an essential role in decoding Ca^{2+} signaling in spines by acting as a leaky Ca^{2+} integrator with the time constant of several seconds. However, the mechanism by which CaMKII α integrates Ca^{2+} signals remains elusive. Here, we imaged CaMKII α -CaM association in single dendritic spines using a new FRET sensor and two-photon fluorescence lifetime imaging. In response to a glutamate uncaging pulse, CaMKII α -CaM association increases in ~ 0.1 s and decays over ~ 3 s. During repetitive glutamate uncaging, which induces spine structural plasticity, CaMKII α -CaM association did not show further increase but sustained at a constant level. Since CaMKII α activity integrates Ca^{2+} signals over ~ 10 s under this condition, the integration of Ca^{2+} signal by CaMKII α during spine structural plasticity is largely due to Ca^{2+} /CaM-independent, autonomous activity. Based on these results, we propose a simple kinetic model of CaMKII α activation in dendritic spines.

¹Department of Biochemistry, Duke University, Durham, NC 27707, USA. ²Neuronal Signal Transduction Group, Max Planck Florida Institute for Neuroscience, Jupiter, FL 33458, USA. Correspondence and requests for materials should be addressed to R.Y. (email: Ryohei.Yasuda@mpfi.org)

Calcium (Ca^{2+})/calmodulin-dependent kinase II (CaMKII), a serine/threonine kinase, is critical for various forms of synaptic plasticity that underlie learning and memory. CaMKII is composed of 12 subunits, each of which is a kinase that is activated by the binding of Ca^{2+} /calmodulin (CaM)¹. The most abundant subunit in the forebrain, CaMKII α , is required for LTP, spine structural LTP (sLTP) and spatial learning^{2–5}. In addition to Ca^{2+} /CaM binding, CaMKII α activity is regulated by autophosphorylation at multiple sites. Autophosphorylation at Thr286 prolongs CaMKII α activity^{6–8}, permitting the integration of Ca^{2+} transients to facilitate the induction of spine plasticity^{9,10}. Disruption of this phosphorylation in *Camk2a*^{T286A} knock-in mice impairs LTP, sLTP, and spatial learning and memory^{10,11}. It is known that phosphorylation at Thr286 causes an enhancement in binding affinity to Ca^{2+} /CaM^{7,12} as well as induces a Ca^{2+} /CaM-independent, autonomous kinase activity state^{13,14}. This autonomous activity of CaMKII α is thought to be important for the induction and the maintenance of LTP¹⁴. CaMKII α is additionally regulated by autophosphorylation at Thr305 and Thr306, which inhibit binding of Ca^{2+} /CaM to CaMKII α ^{15,16}.

CaMKII α activity in response to Ca^{2+} elevations in dendritic spines can be measured by a fluorescence resonance energy transfer (FRET) sensor Camu α in combination with 2-photon fluorescence lifetime imaging (2pFLIM)^{6,10,17}. A brief pulse of two-photon glutamate uncaging induces a transient Ca^{2+} elevation, lasting ~100 ms, in the stimulated spine^{6,10,18}. This causes a rapid CaMKII α activation, which peaks within ~0.5 s and then decays over ~10 s, in the stimulated spine¹⁰. In response to a repetitive glutamate uncaging (~0.5 Hz), which induces LTP in the stimulated spine^{5,6}, CaMKII α activity increases in a step-wise manner, following each uncaging pulse until plateauing within ~10 s (ref. 10). After the cessation of glutamate uncaging, CaMKII α activity decayed with time constants of ~6 s and ~1 min

(ref. 10). These experiments suggest that CaMKII α is a leaky integrator of Ca^{2+} signals¹⁰.

Camu α measures the conformation change of CaMKII α associated with its activation by both Ca^{2+} /CaM binding and Thr286 autophosphorylation^{6,17}. Previous studies using this sensor suggest that the optimal integration of Ca^{2+} signals by CaMKII α requires Thr286 autophosphorylation, suggesting that autonomous activity may play an important role in this process^{6,10}. However, if an autonomous state of CaMKII α exists in the stimulated spines, and if so, how much this state contributes to CaMKII α activation remains elusive.

Here, we used two-photon fluorescence lifetime microscopy (2pFLIM) to probe the association between CaMKII α and Ca^{2+} /CaM. Our results revealed that the fraction of CaMKII α bound to Ca^{2+} /CaM does not continue to increase with multiple Ca^{2+} transients during the induction of sLTP. Taken together with our previous report showing that CaMKII α activity integrates Ca^{2+} signals over ~10 s to 1 min under similar conditions¹⁰, our results suggest that the integration of Ca^{2+} signals depends largely on Ca^{2+} /CaM-independent, 'autonomous' activity of CaMKII α . We propose a simple kinetic scheme of CaMKII α activation that is consistent with our experimental results both for CaMKII α -CaM association and for CaMKII α activation. This model highlights that autonomous activity, but not Ca^{2+} /CaM-dependent activity, accounts for the majority of CaMKII α activity.

Results

Sensor for association of CaMKII α and calmodulin. To measure the association of CaMKII α with CaM, we developed a FRET-based biosensor made of monomeric EGFP (mEGFP)-CaMKII α and mCherry-CaM (Fig. 1a)¹⁹. Biochemical cell-free assays showed that mCherry-CaM supports CaMKII α activity

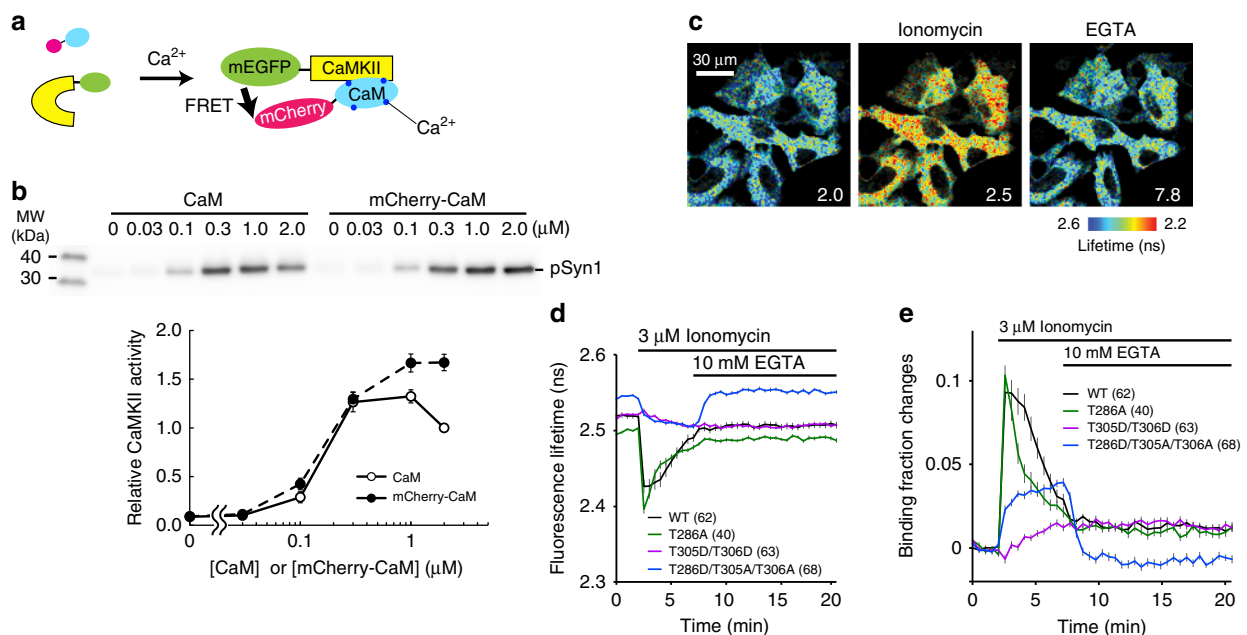


Fig. 1 Design and characterization of CaMKII α -CaM association sensor. **a** Design of a FRET sensor for CaMKII α -CaM association. Monomeric EGFP (mEGFP) and monomeric Cherry (mCherry) fluorescent protein are fused to the N-terminus of CaMKII α and the N-terminus of CaM, respectively. **b** mCherry-CaM activates CaMKII α to the degree similar to non-labeled CaM at different concentrations of CaM in a cell-free system. Upper panel: western blot of phosphorylated Synapsin1 peptide (pSyn1) fused to mCherry. Lower panel: quantification of pSyn1 signal from 4 experiments, normalized with the pSyn1 signal at 2 μM non-labeled CaM. **c** Fluorescence lifetime images of CaMKII α -CaM association sensor expressed in HeLa cells. **d** Time courses of fluorescence lifetime of CaMKII α -CaM association sensor and its mutants (T286A, T305D/T306D and T286D/T305A/T306A) in response to bath application of Ionomycin (3 μM) and EGTA (10 mM). **e** Time courses of changes in CaMKII α -CaM association calculated from **d**. All data are shown in mean \pm sem

similarly to a non-labeled CaM at a wide range of concentrations ($0.03 \mu\text{M} < [\text{CaM or mCherry-CaM}] < 2 \mu\text{M}$) (Fig. 1b), suggesting that mCherry fusion does not affect the affinity of CaM for CaMKII α .

We further characterized the CaMKII α -CaM association sensor in HeLa cells (Fig. 1c–e). To do so, we bath-applied an ionophore (3 μM ionomycin) to elevate intracellular $[\text{Ca}^{2+}]$, and then subsequently added EGTA to reverse the reaction. In response to the ionophore application, the CaMKII α -CaM association sensor first showed a rapid increase in FRET signal, which decayed over a few minutes. This signal further decayed in response to extracellular EGTA application, which chelates extracellular $[\text{Ca}^{2+}]$ (and thus decreasing intracellular $[\text{Ca}^{2+}]$) (Fig. 1c–e). However, we observed a residual CaMKII α -CaM association, which persisted more than 20 min.

Next, we characterized the association of CaM with various CaMKII α phosphorylation mutants. We first introduced phospho-mimic mutations of inhibitory autophosphorylation sites (T305D/T306D) to inhibit the interaction of CaM to the regulatory domain of CaMKII α ^{2,15}. We found that the mutation largely inhibited the rapid CaM binding, consistent with the previous reports¹⁵. However, there was a small and persistent increase in FRET signal, whose amplitude and time scale are similar to that of the persistent component of the FRET signal of wildtype (WT) CaMKII α^{WT} -CaM association. Since the regulatory domain of T305D/T306D mutant does not have the capability to bind $\text{Ca}^{2+}/\text{CaM}$ ^{2,15}, the observed persistent CaMKII α^{WT} -CaM association is unlikely due to the association of CaM to the regulatory domain of CaMKII α . Phospho-dead mutation at Thr286 (T286A), the site important for autonomous CaMKII α activation⁸, accelerated the decay of FRET signal, consistent with a role phosphorylation at this site to prolong CaMKII α activation¹⁰. A small population of CaMKII α^{T286A} mutant also exhibited persistent CaM binding, suggesting that this component is related to neither CaM binding to the regulatory domain nor T286 autophosphorylation, and thus perhaps not related to the regulation of CaMKII α activation. Finally, we measured the binding of CaM with a phospho-mimic mutation at Thr286 (T286D). Since this mutation is known to cause inhibitory autophosphorylation at T305/T306, which inhibits $\text{Ca}^{2+}/\text{CaM}$ binding^{15,16}, we introduced T305A/T306A mutation in addition to T286D (CaMKII $\alpha^{\text{T286D/T305A/T306A}}$)²⁰. In response to ionophore application, CaMKII $\alpha^{\text{T286D/T305A/T306A}}$ -CaM association displayed a persistent increase, which was reversed by EGTA application.

Association of CaMKII α -CaM in dendritic spines. To measure the association of CaMKII α -CaM during the induction of spine plasticity, we biolistically transfected organotypic hippocampal slice cultures of mice with the CaMKII α -CaM association sensor and imaged CA1 pyramidal neurons with 2pFLIM. Structural LTP (sLTP) was induced in a single spine by applying repetitive pulses (0.49 Hz, 30 pulses) of two-photon glutamate uncaging to the spine in the absence of extracellular Mg^{2+} (refs. 5,6).

We first measured CaMKII α -CaM association during sLTP induction with a temporal resolution of 128 ms/frame (Fig. 2a). Binding of CaM to CaMKII α occurs rapidly within 1 frame (128 ms) in the stimulated spine. The binding plateaued with the first glutamate uncaging pulse, and subsequent uncaging pulses did not result in a higher level of CaMKII α -CaM association (Fig. 2b–e). The fractional change in binding of CaMKII α to $\text{Ca}^{2+}/\text{CaM}$ during sLTP induction was independent of the overexpression level (Supplementary Fig. 1). After cessation of glutamate uncaging, CaM dissociated from CaMKII α with the time constant of 3.2 ± 0.7 s. In addition to the fast decay, we observed a persistent component after cessation of uncaging (Fig. 2d, e). This component appeared to be not related to

the binding of $\text{Ca}^{2+}/\text{CaM}$ to the CaM-binding domain of CaMKII α , since a CaMKII α mutant without binding capability (CaMKII $\alpha^{\text{T305D/T306D}}$) also showed this persistent component (Fig. 2f), similarly to the results in HeLa cells (Fig. 1e).

The above experiments were performed at room temperature (25–27 °C). At a near physiological temperature (34–35 °C), $\text{Ca}^{2+}/\text{CaM}$ dissociated faster ($\tau = 0.4 \pm 0.5$ s; Supplementary Fig. 2). The temperature coefficient of the dissociation kinetics was determined to be $Q_{10} = 10.3$.

To determine whether CaMKII α -CaM association showed the integration of multiple uncaging pulses, we compared the binding induced during sLTP (trains of pulses) with the CaMKII α -CaM association in response to a single glutamate uncaging pulse (Fig. 3). Binding of $\text{Ca}^{2+}/\text{CaM}$ to CaMKII α increased rapidly in response to a single uncaging pulse, to a magnitude similar to sLTP-inducing stimulations and then decayed (Fig. 3a–c). The dissociation time constant was obtained as $\tau = 2.9 \pm 0.3$ s (Fig. 3c), a value similar to that obtained after the cessation of sLTP induction (Fig. 2e). The fraction of CaMKII α binding to CaM was similar during trains of glutamate uncaging and in response to a single glutamate uncaging pulse (Fig. 3d). This is a sharp contrast to measurements of the active conformation CaMKII α in spines (Fig. 3e), which shows a slower decay in response to a single uncaging pulse (6.4 ± 0.7 s (74%) and 92.6 ± 50.7 s (26%)), and accumulates to higher levels during trains of uncaging pulses¹⁰.

Role of Thr286 phosphorylation in CaMKII α -CaM association.

It has been reported that the binding affinity of CaMKII α for $\text{Ca}^{2+}/\text{CaM}$ increases by Thr286 phosphorylation⁷. To examine to what degree Thr286 phosphorylation affects the decay kinetics of CaMKII α -CaM interaction, we used a CaMKII α^{T286A} mutant sensor (Fig. 4). To minimize the effects of inter-subunit FRET between mEGFP-CaMKII α^{T286A} and mCherry-CaM bound to the adjacent endogenous wildtype CaMKII, we used hippocampal slices from *Camk2a^{\text{T286A}}* knock-in mice. Thus, in this scheme, all the Thr286 residues in CaMKII α subunits in a holoenzyme are mutated to Ala. We first compared the activation of the T286A mutant to that of mEGFP-CaMKII α^{WT} in response to a single glutamate uncaging pulse (Fig. 4a). We observed that the binding fraction increased to a level similar to that of wildtype, but the dissociation was faster by ~ 3 fold ($\tau = 1.2 \pm 0.1$ s).

Next, we measured CaMKII α^{T286A} -CaM association during sLTP induction (glutamate uncaging at 0.49 Hz) (Fig. 4b, c). Unlike the association of CaMKII α^{WT} with CaM, which plateaued after the first uncaging pulse, the association of CaMKII α^{T286A} with CaM decayed after each uncaging pulse, showing a sawtooth-shaped pattern. However, the peak level of the binding fraction change of CaMKII α^{T286A} -CaM was similar to that of CaMKII α^{WT} -CaM. The dissociation time constant of the CaM-CaMKII α^{T286A} interaction was obtained as $\tau = 1.0 \pm 0.2$ s (0.3 ± 0.1 at 34–35 °C, Supplementary Fig. 2b, $Q_{10} = 4.1$).

We again observed a persistent component in the decay of CaMKII α^{T286A} -CaM association after the train (Fig. 4b). Overall, this component requires neither T286 phosphorylation nor CaM binding to the regulatory domain of CaMKII α .

Inhibitory phosphorylations accelerate CaMKII α inactivation.

Next, we asked how the inhibitory phosphorylation at Thr305 and Thr306 may influence the $\text{Ca}^{2+}/\text{CaM}$ association during spine plasticity induction^{16,21}. To do so, we mutated these phosphorylation sites from Threonine to Alanine and measured CaMKII $\alpha^{\text{T305A/T306A}}$ association with $\text{Ca}^{2+}/\text{CaM}$ in response to glutamate uncaging. Following a single uncaging pulse, the binding fraction change of CaMKII $\alpha^{\text{T305A/T306A}}$ with $\text{Ca}^{2+}/\text{CaM}$ increased to a level similar to that of CaMKII α^{WT} but with a

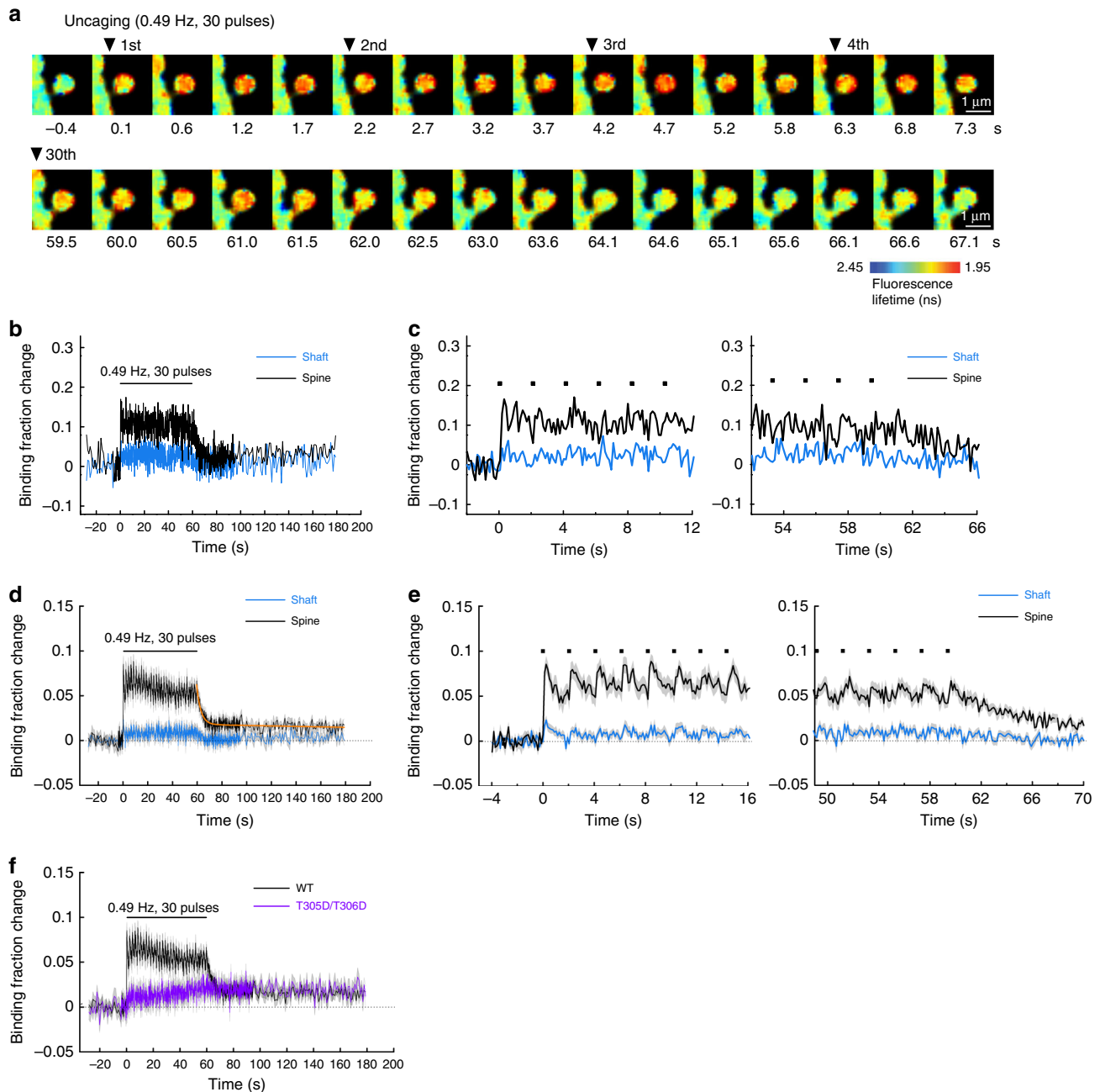


Fig. 2 CaMKII α -CaM association during sLTP induction. **a** Representative fluorescence lifetime images of CaMKII α -CaM association sensor during glutamate uncaging at 0.49 Hz. Warmer colors indicate lower fluorescence lifetime, corresponding to a higher binding fraction of mCherry-CaM to mEGFP-CaMKII α . Scale bar, 1 μ m. **b** Time course of CaMKII α -CaM association in a stimulated spine (black) and nearby dendrite (blue). Analyzed from images in **a**. Black dots represent uncaging pulses. **c** Expanded view of the rising phase (left) and the decay phase (right) of **b**. **d** Averaged change in CaMKII α -CaM association in stimulated spines (black) and nearby dendrite (blue) ($n = 27$ spines/9 neurons). The orange curve indicates the decay of binding fraction change obtained by curve fitting of a double-exponential function: $B(t) = B_0 [P_{fast} \exp(-t/\tau_{fast}) + P_{slow} \exp(-t/\tau_{slow})]$, where B_0 is the initial binding fraction change, τ_{fast} and τ_{slow} are the fast and slow decay time constants and P_{fast} and P_{slow} are the respective populations. The time constants are obtained as $\tau_{fast} = 3.2 \pm 0.6$ s ($P_{fast} = 71\%$) and $\tau_{slow} = 572 \pm 843$ s ($P_{slow} = 29\%$). **e** Expanded view of the rising phase (left) and the decay phase (right) of **d**. **f** Average time course of CaMKII α -CaM association for a mutant mEGFP-CaMKII $\alpha^{T305D/T306D}$ in which the Thr305 and Thr306 are mutated to aspartate. The mutation precludes Ca²⁺/CaM binding in the stimulated spine during glutamate uncaging at 0.49 Hz (purple; $n = 34$ spines/5 neurons). The data for CaMKII α^{WT} (black) are from **c** for the comparison. All data are shown in mean \pm sem, and sem of time constants is obtained by bootstrapping

slightly slower decay ($\tau = 7.5 \pm 1.1$ s; Fig. 5a). During repetitive glutamate uncaging at 0.49 Hz (sLTP protocol), Ca²⁺/CaM binding to CaMKII $\alpha^{T305A/T306A}$ increased to the level similar to that of CaMKII α^{WT} (Fig. 4b) and decayed with the time constant of $\tau = 9.3 \pm 1.8$ s (Fig. 5b, c), which was, again, slower than that of CaMKII α^{WT} ($\tau \sim 3$ s). These results suggested that inhibitory

phosphorylation at Thr305/Thr306 dynamically occurs during CaMKII α activation, which inhibits the rebinding of Ca²⁺/CaM on CaMKII α . However, preventing this regulation during the induction of sLTP (enhancing binding affinity to Ca²⁺/CaM) did not result in a higher level of Ca²⁺/CaM binding.

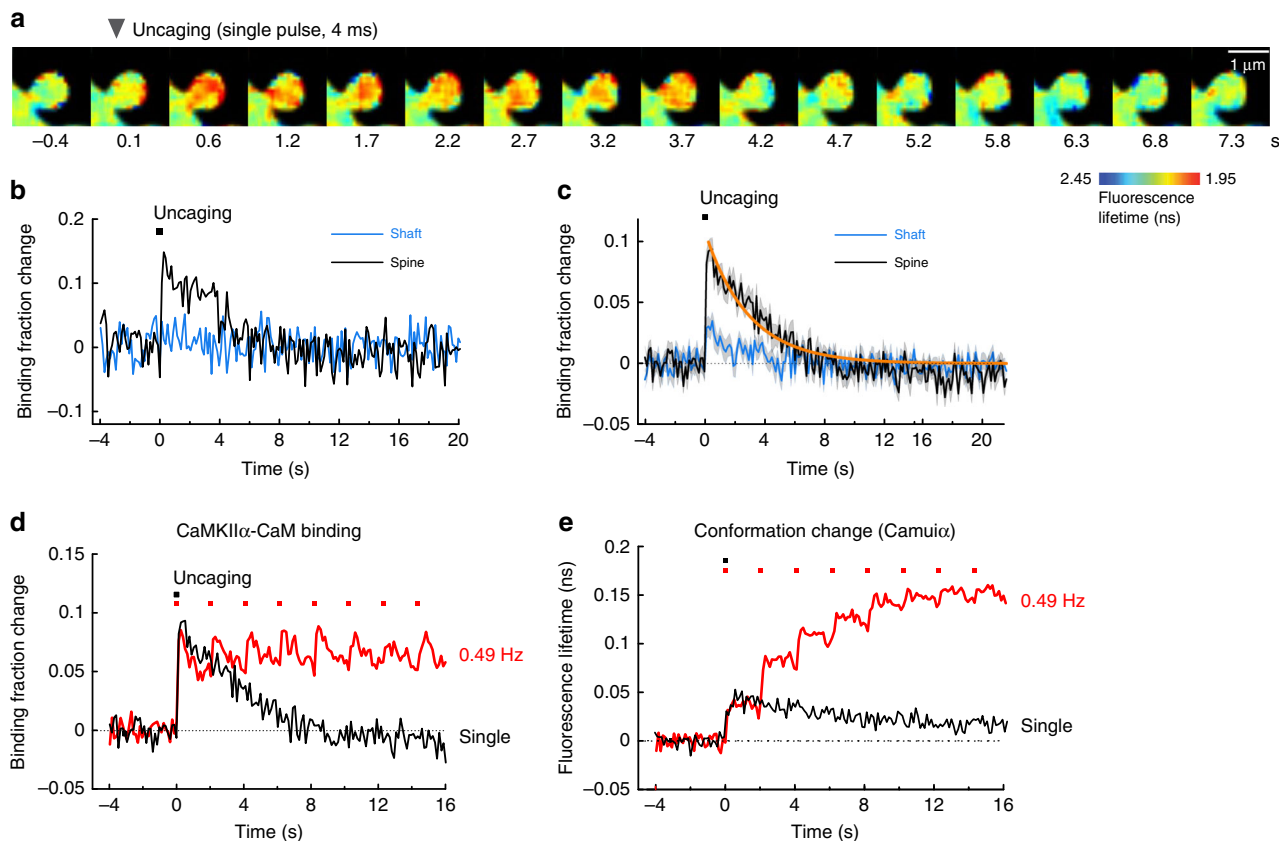


Fig. 3 CaMKII α -CaM association in response to a single glutamate uncaging pulse. **a** Representative fluorescence lifetime images of CaMKII α -CaM association in response to a single glutamate uncaging pulse. Warmer colors indicate lower fluorescence lifetime, corresponding to a higher binding fraction of mCherry-CaM to mEGFP-CaMKII α . Scale bar, 1 μ m. **b** Time course of CaMKII α -CaM association in a stimulated spine (black) and nearby dendritic (blue). Inset is an expanded view of the rising phase. Black squares denote uncaging pulses. Analyzed from images in **a**. **c** Averaged changes in CaMKII α -CaM association in spines and nearby dendrite ($n = 28$ spines/4 neurons). The orange curve indicates the decay of binding fraction change obtained by curve fitting of an exponential function: $B(t) = B_0 \exp(-t/\tau)$, where B_0 is the initial binding fraction change, τ is the dissociation time constant. The time constant is obtained as $\tau = 2.9 \pm 0.3$ s. **d** Comparison of CaMKII α -CaM association in response to a single pulse (**c**) and to a train of glutamate uncaging (Fig. 2d, e). **e** CaMKII α conformation change measured with Green-Camuia α in response to a single pulse and a train of glutamate uncaging. Data from our previous publication¹⁰. All data are shown in mean \pm sem, and sem of time constants is obtained by bootstrapping

A kinetic model of CaMKII α activation. Our results indicated that CaMKII-CaM association was rapidly activated by a single glutamate uncaging pulse, but did not show any integration over repetitive glutamate uncaging (Fig. 3d). In contrast, CaMKII α activity measured with Camuia under similar conditions showed a high degree of integration¹⁰ (Figs. 3e, 6a). The plot assumes that the active population of CaMKII α is equal to the fraction of CaMKII α bound to Ca²⁺/CaM after the first pulse of glutamate. Since CaMKII α autonomous activation is defined by active CaMKII α without CaM binding, this population should be obtained by subtracting the fraction of CaMKII α bound to CaM from CaMKII α activity (cyan area, Fig. 6a). This suggests that CaMKII α activity during sLTP is almost entirely supported by autonomous CaMKII α activation.

To further clarify this point, we created a simple kinetic model of CaMKII α (Fig. 6b, c). We constructed a set of rate equations to describe CaMKII α biochemical reactions based on the proposed model (Table 1), and simulated the reaction in response to repetitive glutamate uncaging induced Ca²⁺ transients at 0.49 Hz, our standard sLTP protocol (Fig. 6b, c). For Ca²⁺-CaM-CaMKII α interaction, we used a model previously established based on biochemical experiments²² (Table 1). When two adjacent subunits are activated, CaMKII α subunit (K) undergoes phosphorylation (P). We assume that the rate of phosphorylation (k_1) is proportional to the chance that the adjacent subunit is active:

the fraction of CaM-bound, unphosphorylated form (KCAM), plus CaM-bound, phosphorylated form (PCaM), plus phosphorylated subunit (P and P₂; see below for the explanation of the P₂ state). The maximum rate has been reported to be 6.3 s⁻¹ (ref. 23), but we found that a two-fold higher value (12.6 s⁻¹) fits our data better. Following previous kinetic models^{22,23}, we assume that CaM rebinding to the P state (P \rightarrow PCaM) and dephosphorylation while the subunit bound to CaM (PCaM \rightarrow KCaM) do not occur. The rate of CaM dissociation from PCaM (k_2) was measured to be 1/3 s⁻¹ (or time constant of 3 s) in this study (Fig. 1), and the rate of dephosphorylation of CaMKII α (k_3) has been previously measured to be 1/6 s⁻¹ (or time constant of 6 s; Chang et al.). In addition, we assume that the persistent component of the FRET signal of CaMKII α -CaM association is not related to the activation of CaMKII α , as it is sensitive neither to T286A mutation nor to T305D/T306D mutations. However, the slow component of CaMKII α activation measured with Camuia (time constant \sim 1 min) depends on T286 phosphorylation, and thus likely represents the autophosphorylation state of CaMKII α ¹⁰. To explain this component of decay in CaMKII α activation, we included a slow phosphorylation state (P₂) with the time constant of 1 min ($k_5 = 1/60$ s⁻¹). The fraction of slow component of CaMKII α activation (\sim 25%; Chang et al.) can be approximated by the ratio of k_3 and k_4 , we set k_3 to be 0.25 k_4 ($k_4 = 0.25/6$ s⁻¹). Overall, we obtained most of the kinetic

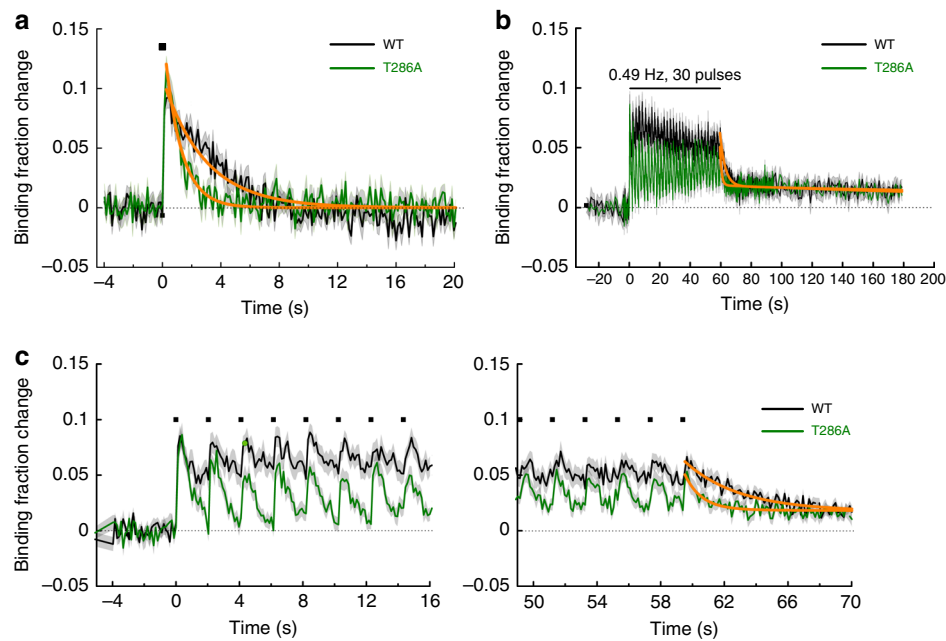


Fig. 4 CaMKII α^{T286A} -CaM association during sLTP induction. **a** Averaged change in CaMKII α^{T286A} -CaM association in a stimulated spine (green; $n = 18$ spines/4 neurons) in response to a single glutamate uncaging pulse (black square). The orange curve on CaMKII α^{T286A} is obtained by curve fitting of an exponential function: $B(t) = B_0 \cdot e^{-t/\tau}$. The dissociation time constant is obtained as $\tau = 1.2 \pm 0.1$ s. The data and fitted curve for CaMKII α^{WT} are from Fig. 3c for the comparison. **b** Averaged change in CaMKII α^{T286A} -CaM association in stimulated spines (green; $n = 24$ spines/7 neurons) during glutamate uncaging at 0.49 Hz. The orange curve indicates the decay of binding fraction change obtained by curve fitting of a double-exponential function: $B(t) = B_0 [P_{fast} \cdot \exp(-t/\tau_{fast}) + P_{slow} \cdot \exp(-t/\tau_{slow})]$. The time constants for CaMKII α^{T286A} are obtained as $\tau_{fast} = 1.0 \pm 0.2$ s ($P_{fast} = 63\%$) and $\tau_{slow} = 356 \pm 221$ s ($P_{slow} = 37\%$). The data and fitted curve for CaMKII α^{WT} (black) are from Fig. 2d for the comparison. **c** Expanded view of the initial phase (left) and the late phase (right) of plot in **b**. All data are shown in mean \pm sem, and sem of time constants is obtained by bootstrapping

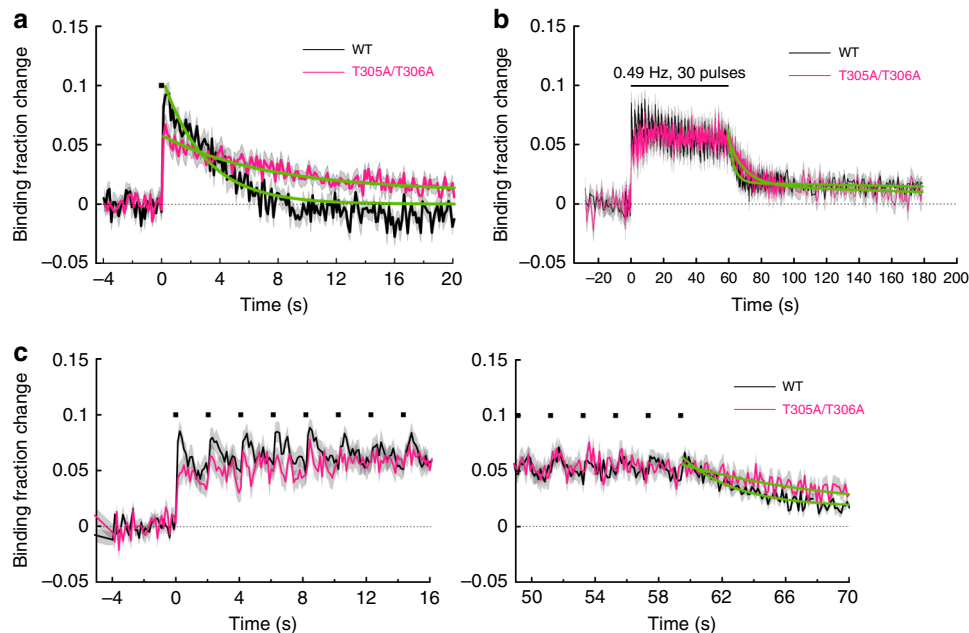


Fig. 5 Association of CaMKII $\alpha^{T305A/T306A}$ -CaM during sLTP induction. **a** Averaged change in CaMKII $\alpha^{T305A/T306A}$ -CaM association in a stimulated spine (magenta; $n = 34$ spines/6 neurons) in response to a single glutamate uncaging pulse (black square). The green curve on CaMKII $\alpha^{T305A/T306A}$ is obtained by curve fitting of an exponential function: $B(t) = B_0 \exp(-t/\tau)$. The dissociation time constant is obtained as $\tau = 7.5 \pm 1.1$ s. Inset is an expanded view. The data and fitted curve for CaMKII α^{WT} are from (Fig. 3c) for the comparison. **b** Averaged change in CaMKII $\alpha^{T305A/T306A}$ -CaM association ($n = 27$ spines/8 neurons) during glutamate uncaging at 0.49 Hz. The green curve indicates the decay of binding fraction change obtained by curve fitting of a double-exponential function: $B(t) = B_0 [P_{fast} \cdot \exp(-t/\tau_{fast}) + P_{slow} \cdot \exp(-t/\tau_{slow})]$. The time constants are obtained as $\tau_{fast} = 9.3 \pm 1.8$ s ($P_{fast} = 71\%$) and $\tau_{slow} = 249 \pm 229$ s ($P_{slow} = 29\%$). The data and fitted curve for CaMKII α^{WT} are from (Fig. 2d) for the comparison. **c** Expanded view of the initial phase (left) and the late phase (right) in **b**

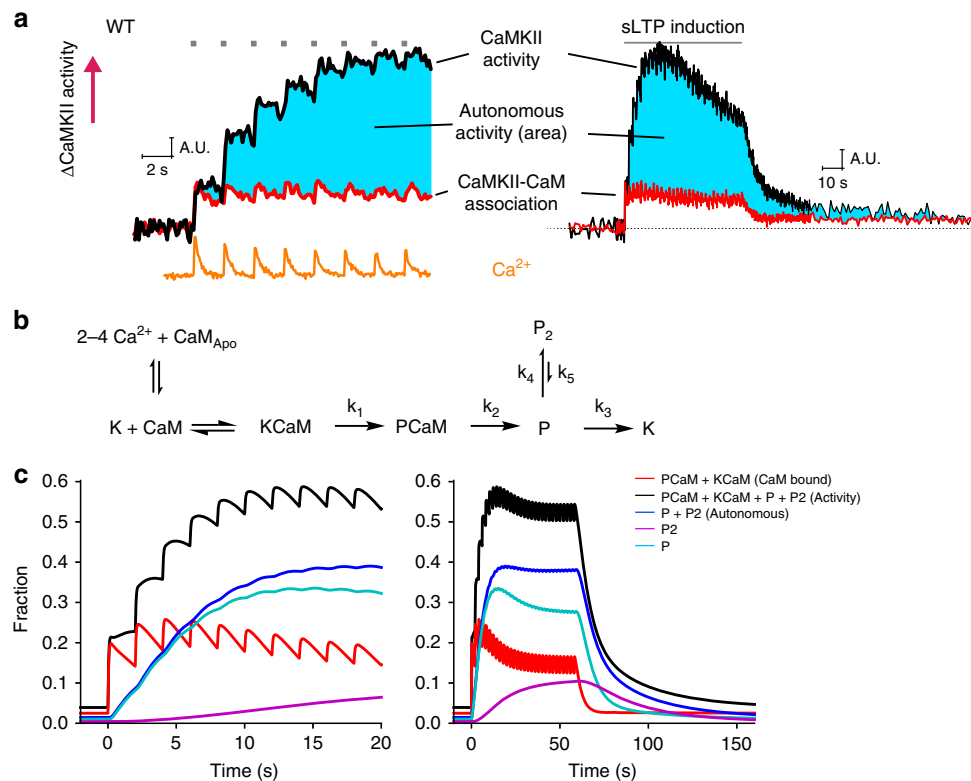


Fig. 6 Simulated CaMKII α activation during spine plasticity induction. **a** The comparison of CaMKII α activity measured with Green-Camuia (data from ref. ¹⁰), Ca^{2+} measured with Fluo-4FF (data from ref. ¹⁰), and CaMKII α -CaM association measured in this study. Autonomous activity is the subtraction of CaMKII α -CaM association from CaMKII α activation (cyan). The first time point right after uncaging is matched for CaMKII α -CaM and CaMKII α activity, assuming that there is no autonomous CaMKII α at the time point. **b** Reaction scheme of CaMKII α activation. K is the inactive state of CaMKII α (closed form), CaM_{Apo} is the inactive form of calmodulin without bound Ca^{2+} , CaM is the active form of calmodulin with 2–4 bound Ca^{2+} ions, P and P₂ are the two different states of Thr286-phosphorylated CaMKII α . **c** Simulated CaMKII α activation based on the proposed reaction scheme. Black: concentration of total active CaMKII α (KCaM + PCaM + P + P₂). Red: concentration of KCaM and PCaM. Green: concentration of Thr286-phosphorylated CaMKII α (P + P₂). Light blue: concentration of P state of CaMKII α . Navy: concentration of P₂ state of CaMKII α .

parameters necessary for simulating the reaction (parameters for CaM association and k_1 – k_5 in Fig. 6b) from this and previous studies^{10,22} (Table 1).

This reaction scheme recapitulates several key features of CaMKII α activation and CaM-CaMKII α binding in single dendritic spines: (1) decay kinetics of CaMKII α activation with two time constants¹⁰, (2) integration of CaMKII α activation in response to each pulse¹⁰, (3) no accumulation of CaMKII α -CaM interaction during repetitive Ca^{2+} pulses, (4) decay of CaMKII α activity in response to a single pulse (~10 s), which is longer than that following a train of pulses (~6 s)¹⁰, (5) time course of CaM binding to T286A mutant, simulated by removing the effects of phosphorylation (setting k_1 to 0). The model shows that autonomous CaMKII α activation (P + P₂) increases over time, and becomes the dominant population after ~3–4 uncaging pulses.

Previously our and other groups examined the effects of Thr286 dephosphorylation on CaMKII α activity using Camuia sensor with T286D mutation or wildtype Camuia sensor in the presence of phosphatase inhibitor^{10,24}. These studies showed a high basal level of CaMKII α activity before glutamate uncaging, consistent with this study that T286 phosphorylation accounts for most of CaMKII α activation. Interestingly, both studies showed that there exists a smaller, rapid increase of active CaMKII α which decays rapidly after cessation of glutamate uncaging. Since the phosphorylation state of T286 is constantly in “on” state under this condition, this rapid activation must be due to the association/dissociation of Ca^{2+} /CaM from CaMKII α ^{T286D}.

To simulate the activation of CaMKII α ^{T286D}, we slightly modified the above model. First, we allowed phosphorylated CaMKII α binds to CaM (P \rightarrow PCaM) with 10% of the association rate of non-phosphorylated K-CaM with CaM (K \rightarrow KCaM). Second, we assumed that CaMKII α activity in the autonomous state (P or P₂) is 60% as high as that when binding with CaM (KCaM or PCaM), as measured previously with FRET sensors^{6,17} and substrate phosphorylation²⁵ (Fig. 7a). This model produced a time course of CaMKII α ^{WT} activation similar to that produced by the original model (Fig. 7b). Importantly, when we set dephosphorylation rate to zero to simulate T286D mutation, we recapitulated all above features of CaMKII α ^{T286D} activity^{10,24} (Fig. 7b, c), including high basal activity and a rapid activation and inactivation due to CaM binding and unbinding, respectively. The same model also reproduced the activity profile of T286A mutation (set the rate of phosphorylation to 0), showing smaller basal activity, smaller activation, and faster decay¹⁰ (Fig. 7b, c).

Finally, we examined how this model predicts CaMKII α activation during spike-timing-dependent plasticity (STDP), in which LTP can be induced by pairing synaptic stimulation with back-propagating action potentials (bAP) with slight delay²⁶. We assumed that bAPs produce Ca^{2+} transient with the peak concentration of 0.8 μM and the decay time constant of 20 ms^{27,28}. When paired with synaptic release at the synapse, ~3 times more Ca^{2+} is produced²⁹. In this model, bAPs alone produced little CaMKII α activation (Fig. 7d). However, when paired with synaptic activity, the stimulation activated CaMKII α to a higher level, reaching the level similar to that produced

Table 1 List of parameters used for simulation

Name	Meaning	Value (Rate constant or concentration)	Note	
CaM	Calmodulin			
CaM _{Apo}	Calmodulin without bound Ca ²⁺			
Ca(n)CaM-C	Calmodulin binding n Ca ²⁺ on its C-lobe			
Ca(n)CaM-N	Calmodulin binding n Ca ²⁺ on its N-lobe			
Ca4CaM	Calmodulin binding 4 Ca ²⁺			
KCaM	CaMKIIα without T286 phosphorylation bound to CaM			
K	CaMKIIα without T286 phosphorylation			
P	CaMKIIα with Thr286 phosphorylation			
P ₂	A different form of CaMKIIα with Thr286 phosphorylation			
KCaM	K associated with CaM			
PCaM	P associated with CaM			
F	Fraction of active CaMKII subunits, KCaM + PCaM + P + P ₂			
CaM1C _{on}	Ca ²⁺ + CaM _{Apo} → CaCaM-C	5 × 10 ⁶ M ⁻¹ s ⁻¹	Values from Pepke et al. ²²	
CaM1C _{off}	CaCaM-C → Ca ²⁺ + CaM _{Apo}	50 s ⁻¹		
CaM2C _{on}	Ca ²⁺ + CaCaM-C → Ca2CaM-C	10 × 10 ⁶ M ⁻¹ s ⁻¹		
CaM2C _{off}	Ca2CaM-C → Ca ²⁺ + CaCaM-C	10 s ⁻¹		
CaM1N _{on}	Ca ²⁺ + CaM _{Apo} → CaCaM-N	100 × 10 ⁶ M ⁻¹ s ⁻¹		
CaM1N _{off}	CaCaM-N → Ca ²⁺ + CaM-N	2 × 10 ³ s		
CaM2N _{on}	Ca ²⁺ + CaCaM-N → Ca2CaM-N	200 × 10 ⁶ M ⁻¹ s ⁻¹		
CaM2N _{off}	Ca2CaM-N → Ca ²⁺ + Ca2CaM	500 s ⁻¹		
KCaM1C _{on}	Ca ²⁺ + KCaM _{Apo} → KCaCaM-C	44 × 10 ⁶ M ⁻¹ s ⁻¹		
KCaM1C _{off}	KCaCaM-C → Ca ²⁺ + KCaM _{Apo}	33 s ⁻¹		
KCaM2C _{on}	Ca ²⁺ + KCaCaM-C → KCa2CaM-C	44 × 10 ⁶ M ⁻¹ s ⁻¹		
KCaM2C _{off}	KCa2CaM-C → Ca ²⁺ + KCaCaM-C	0.8 s ⁻¹		
KCaM1N _{on}	Ca ²⁺ + KCaM _{Apo} → KCaCaM-N	76 × 10 ⁶ M ⁻¹ s ⁻¹		
KCaM1N _{off}	KCaCaM-N → Ca ²⁺ + KCaM _{Apo}	300 s ⁻¹		
KCaM2N _{on}	Ca ²⁺ + KCaCaM-N → KCa2CaM-N	76 × 10 ⁶ M ⁻¹ s ⁻¹		
KCaM2N _{off}	KCa2CaM-N → Ca ²⁺ + KCaCaM-N	20 s ⁻¹		
R1	2 Ca ²⁺ + CaM _{Apo} → Ca2CaM-C	$\frac{CaM1C_{on} \cdot CaM2C_{on}}{CaM1C_{off} + CaM2C_{on}} [Ca^{2+}]$		Coarse grained model by Pepke et al. ²² for R1-R24
R2	Ca2CaM-C → 2 Ca ²⁺ + CaM _{Apo}	$\frac{CaM1C_{off} \cdot CaM2C_{off}}{CaM1C_{off} + CaM2C_{on}} [Ca^{2+}]$		
R3	2 Ca ²⁺ + CaM _{Apo} → Ca2CaM-N	$\frac{CaM1N_{on} \cdot CaM2N_{on}}{CaM1N_{off} + CaM2N_{on}} [Ca^{2+}]$		
R4	Ca2CaM-N → 2 Ca ²⁺ + CaM _{Apo}	$\frac{CaM1N_{off} \cdot CaM2N_{off}}{CaM1N_{off} + CaM2N_{on}} [Ca^{2+}]$		
R5	2 Ca ²⁺ + Ca2CaM-C → Ca4CaM	Same as R3		
R6	Ca4CaM → 2 Ca ²⁺ + Ca2CaM-C	Same as R4		
R7	2 Ca ²⁺ + Ca2CaM-N → Ca4CaM	Same as R1		
R8	Ca4CaM → 2 Ca ²⁺ + Ca2CaM-N	Same as R2		
R9	2 Ca ²⁺ + KCaM _{Apo} → KCa2CaM-C	$\frac{KCaM1C_{on} \cdot KCaM2C_{on}}{KCaM1C_{off} + KCaM2C_{on}} [Ca^{2+}]$		
R10	KCa2CaM-C → 2 Ca ²⁺ + KCaM _{Apo}	$\frac{KCaM1C_{off} \cdot KCaM2C_{off}}{KCaM1C_{off} + KCaM2C_{on}} [Ca^{2+}]$		
R11	2 Ca ²⁺ + KCaM _{Apo} → KCa2CaM-N	$\frac{KCaM1N_{on} \cdot KCaM2N_{on}}{KCaM1N_{off} + KCaM2N_{on}} [Ca^{2+}]$		
R12	KCa2CaM-N → 2 Ca ²⁺ + KCaM _{Apo}	$\frac{KCaM1N_{off} \cdot KCaM2N_{off}}{KCaM1N_{off} + KCaM2N_{on}} [Ca^{2+}]$		
R13	2 Ca ²⁺ + KCa2CaM-C → KCa4CaM	Same as R11		
R14	KCa4CaM → 2 Ca ²⁺ + KCa2CaM-C	Same as R12		
R15	2 Ca ²⁺ + KCa2CaM-N → KCa4CaM	Same as R9		
R16	KCa4CaM → 2 Ca ²⁺ + KCa2CaM-N	Same as R10		
R17	K + CaM _{Apo} → KCaM _{Apo}	3.8 × 10 ³ M ⁻¹ s ⁻¹		
R18	KCaM _{Apo} → K + CaM _{Apo}	5.5 s ⁻¹		
R19	K + Ca2CaM-C → KCa2CaM-C	0.92 × 10 ³ M ⁻¹ s ⁻¹		
R20	KCa2CaM-C → K + Ca2CaM-C	6.8 s ⁻¹		
R21	K + Ca2CaM-N → KCa2CaM-N	0.12 × 10 ³ M ⁻¹ s ⁻¹		
R22	KCa2CaM-N → K + Ca2CaM-N	1.7 s ⁻¹		
R23	K + Ca4CaM → KCa4CaM	30 × 10 ³ M ⁻¹ s ⁻¹		
R24	KCa4CaM → K + Ca4CaM	1.5 s ⁻¹		
R25	KCaM → PCaM	k _i : F × 12.6 s ⁻¹	6.3 according to Lucic et al., ²³ F is the fraction of active CaMKII subunits	
R26	PCaM → P + CaM	k ₂ : 0.33 s ⁻¹	Decay of Ca ²⁺ -CaMKII association, 3 s.	
R27	P → P ₂	k ₄ : 0.041 s ⁻¹	k ₃ /k ₄ = 1/4: the fraction of slow component	
R28	P ₂ → P	k ₅ : 0.017 s ⁻¹	Slow decay of CaMKII: 60 s Chang et al. ¹⁰	
R29	P → K	k ₃ : 0.17 s ⁻¹	Fast decay of CaMKII activity: 6 s (ref. 10)	
R30 - R33	Same as R17, R19, R21, R23, with K replaced by P	0.1 × R17, R19, R21, R23 for the model in Fig. S3a and 0 for the model in Fig. 6a	Ca ²⁺ /CaM binding to phosphorylated CaMKII (P)	
R34 - R41	Same as R9 - R16, with K replaced by P	Same as R9 - R16.	Ca ²⁺ binding to CaM on P	
[Ca ²⁺] _{peak}	Peak [Ca ²⁺]	4 μM for uncaging, 0.8 μM for back-propagating action potential (bAP), 2.4 μM for bAP paired with synaptic stimulation.	Evans et al., ³⁹ Chang et al., ¹⁰ Sabatini et al. ²⁷	
τ _{Ca}	Decay of Ca ²⁺	100 ms for uncaging, 20 ms for bAP and bAP paired with synaptic stimulation.	Evans et al., ³⁹ Chang et al., ¹⁰ Sabatini et al. ²⁷	
[Ca ²⁺] ₀	Resting [Ca ²⁺]	50 nM	Evans et al., ³⁹ Chang et al., ¹⁰ Sabatini et al. ²⁷	
CaM _T	Total calmodulin concentration	30 μM	Pepke et al., ²² Kakiuchi et al. ⁴¹	
CaMKII _T	Total CaMKII subunit concentration	70 μM	Pepke et al., ²² Lee et al. ⁶	

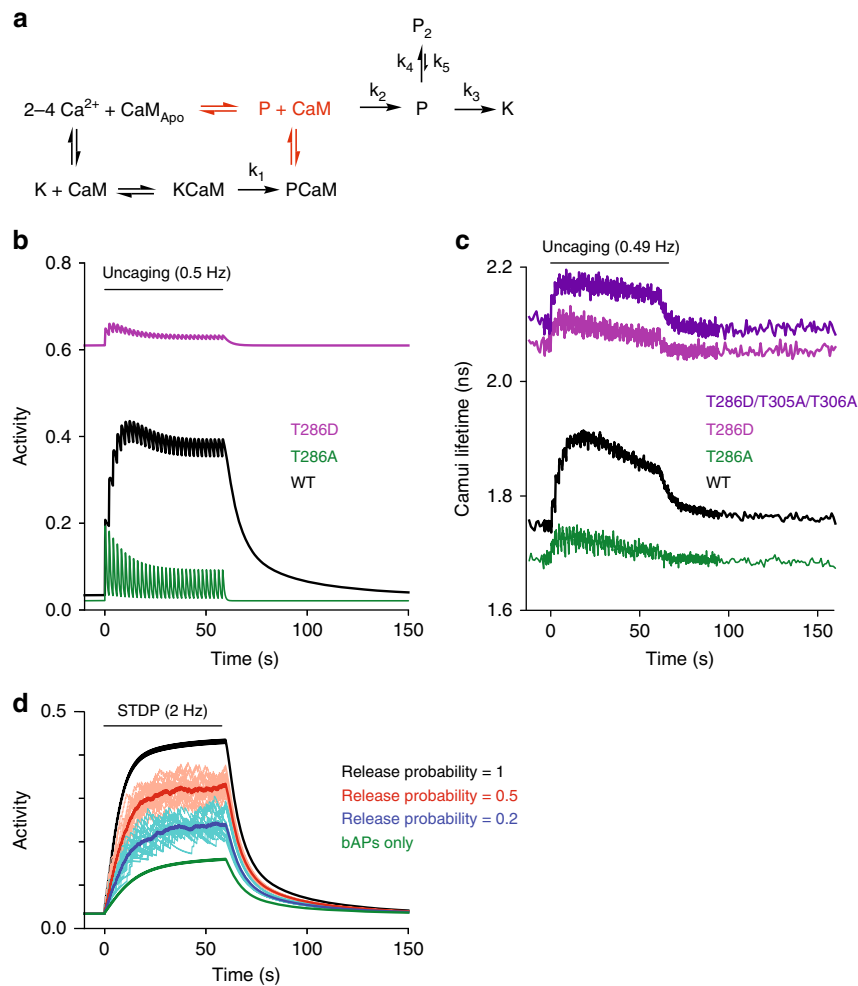


Fig. 7 Modified model of CaMKII α activation during spine plasticity induction. **a** Reaction scheme of CaMKII α activation that includes binding of CaM to phosphorylated CaMKII α (P state). The difference from Fig. 6b is highlighted in red. **b** Simulated activation of CaMKII α with mutations at T286 based on the proposed reaction scheme (a). Black: wildtype, green: T286A mutant, purple: T286D mutant, dark blue: T286D/T305A/T306A mutant. T305A/T306A mutations are to prevent inhibition of CaM binding to T286D mutant by inhibitory T305/T306 phosphorylations²⁴. **c** Activation of CaMKII α and its mutants in dendritic spines measured with Green-Camuix (data from ref. 10). **d** Simulated CaMKII α during a protocol to induce spike-timing-dependent plasticity (2 Hz pairing of synaptic stimulation and back-propagating action potentials)

by glutamate uncaging, particularly at high presynaptic release probability (Fig. 7d).

Discussion

The fraction of CaMKII α bound to Ca²⁺/CaM remains constant during repetitive uncaging pulses, and does not increase with each additional Ca²⁺ transient. This temporal pattern is sharply contrasted by the stepwise activation of CaMKII α observed with the conformational sensor, Camuix¹⁰. This suggests that CaM-independent CaMKII α activation, i.e., autonomous activation, is the dominant mechanism that causes the accumulation of CaMKII α activity during the induction of sLTP. These results highlight the important role of autonomous activation by the phosphorylation of Thr286 plays in the induction of synaptic plasticity¹⁰.

In the absence of Thr286 phosphorylation (T286A), the association of CaMKII α ^{T286A}-CaM showed a transient binding during sLTP induction, which was similar to Camuix^{T286A} activation¹⁰. Thus, the activation of CaMKII α ^{T286A} is mediated by the transient binding of Ca²⁺/CaM ($\tau \sim 1$ s). In addition, from the decay rate, we found that the decay time constant between T286A is ~ 3 times faster than wildtype, suggesting that Thr286

phosphorylation slows down the dissociation rate. It has been reported that the binding affinity of CaMKII α for Ca²⁺/CaM is enhanced by orders of magnitude upon Thr286 phosphorylation in cuvette^{7,12}. However, the obtained decay rates suggest that the enhancement is only a few folds in the spine.

In addition to Thr286, CaMKII α undergoes autophosphorylation at Thr305 and Thr306 upon its activation. Phosphorylation of these sites is known to inhibit CaM binding to CaMKII^{16,21}. Consistent with these previous studies, our imaging results indicate that the dissociation of CaM from CaMKII α is slower when this phosphorylation is prevented by mutations of Thr305 and Thr306 to Ala. Transgenic CaMKII α ^{T305V/T306A} mice have been shown to have a lower threshold for hippocampal LTP². The longer activity of CaMKII α ^{T305A/T306A} suggests that there might be a less stringent window in LTP stimulation frequency required for LTP induction in transgenic CaMKII α ^{T305V/T306A} mice.

Taken together with our previous studies of CaMKII α activation during repetitive Ca²⁺ pulses in the spine^{6,10}, CaMKII α activation, but not CaMKII α -CaM binding, integrates Ca²⁺ pulses. This suggests that most of the active CaMKII α population is in a CaM-independent, autonomous activation state. Our kinetic model also predicts that the CaMKII α bound to CaM accounts

for only a small fraction of CaMKII α activity (~1/4), and most of the activity is from autonomous activation.

We propose a slow state in Thr286-phosphorylated CaMKII α (P_2) to explain the minor population (~25%) with a long decay time of CaMKII α activity (~60 s)¹⁰. However, there would be different ways to explain this fraction. For example, it could also possibly originate from two different types of phosphatases which target different populations of CaMKII α ^{30,31}. Further experiments are required to disentangle these two different states.

For the simulation of T286D mutant (or phosphor-mimic) form of CaMKII α , we needed to modify the model so that it incorporates the binding of CaM to the phosphorylated form of CaMKII α . While some of the previously developed models ignore this reaction³², it would be valid since our experiments in HeLa cells clearly shows CaM binding to T286D mutant. In addition, we incorporated the previous measurements suggesting that the CaM-bound form is higher than autonomous activity^{6,17,25}. This modified model recapitulated the reported time course of CaMKII α ^{T286D} in single spines: high basal binding, rapid activation, and rapid inactivation^{10,24}. Importantly, the rapid inactivation of CaMKII α ^{T286D} has been used to challenge the idea that the decay of CaMKII α is due to dephosphorylation of CaMKII α ²⁴. However, our simulation indicates that, while the decay of CaMKII α ^{T286D} is due to unbinding of CaM, that of wildtype CaMKII α is limited mostly by dephosphorylation of the autonomous form.

Finally, the model does not explicitly incorporate several factors including caching of CaM by neurogranin, cooperativity between subunits and inhibitory autophosphorylation at Thr305/Thr306^{23,32–34}. Perhaps the more detailed model based on CaMKII α structure and biochemical data together with our imaging results in dendritic spines would improve our understanding of CaMKII α activation in dendritic spines in response to Ca²⁺ elevation^{33,35}.

Methods

Experimental animals. Mice from BL6/C57 strain (purchased from Charles River Laboratories) were used for CaMKII α ^{WT}-CaM association measurements in 2pFLIM imaging. *Camk2a*^{T286A} knock-in mice (gift from Dr. Giese) were used for CaMKII α ^{T286A}-CaM association measurements. All experimental animals were bred in-house under the guidelines of Institutional Animal Care and Use Committee (IACUC) of Duke University Medical Center and Max Planck Florida Institute for Neuroscience.

Organotypic slices. Organotypic cultured hippocampal slices were prepared from postnatal 4–7 day mice³⁶. The isolated hippocampus was sliced with a tissue chopper (McIlwain Tissue Chopper, Ted Pella Inc). The slices were plated on cell culture inserts (hydrophilic PTFE, 0.4 μ m, Millipore) and maintained in tissue medium (minimum essential medium Eagle (MEM) 8.4 mg/ml, horse serum 20%, L-glutamine 1 mM, CaCl₂ 1 mM, MgSO₄ 2 mM, D-glucose 12.9 mM, NaHCO₃ 5.2 mM, HEPES 30 mM, insulin 1 μ g/ml, ascorbic acid 0.075%) at 37 °C supplemented with 5% CO₂ until experiments (DIV 12–19). Hippocampal slices were biologically transfected with plasmids at DIV 5–10 (12 mg gold particle, size: 1 μ m, 45–112 μ g plasmid). Preparation of slice cultures was in accordance with the guidelines of the Institutional Animal Care and Use Committee of Duke University Medical Center and Max Planck Florida Institute for Neuroscience.

Cell lines. HeLa cells (ATCC, Cat#CCL-2) were cultured in Dulbecco's modified Eagle medium supplemented with 10% fetal bovine serum at 37 °C in 5% CO₂. Cells were transfected with mCherry-CaM and mEGFP-CaMKII α (or its mutant) using Lipofectamine-2000 for 24–48 h, and subjected to fluorescence lifetime imaging in a solution containing (in mM) 130 NaCl, 20 HEPES, 2 NaHCO₃, 25 D-glucose, 2.5 KCl, 1.25 NaH₂PO₄, 0.8 MgCl₂ and 1.8 mM CaCl₂ (pH 7.3). Cells were treated with 3 μ M ionomycin (Tocris) and then 5 min later 10 mM EGTA (Sigma).

Protein purification. His-tagged mCherry-synapsin 1 peptide (a gift from Dr. Murakoshi)³⁷, His-tagged mCherry-CaM and His-tagged calmodulin were cloned into pRSET bacterial expression vector (Thermo Fisher Scientific) and expressed in T7 Express *lysY* Competent *Escherichia Coli* (New England BioLabs Inc.), purified with a Ni-NTA column (HisTrap™ HP; GE Healthcare) and desalted with PD-10 column (GE Healthcare). The purified protein concentrations were measured by

Pierce™ BCA Protein Assay Kit (Thermo Fisher Scientific). The purity of each fraction was confirmed by SDS-PAGE and Coomassie staining.

Kinase assay. Standard kinase assays were performed for the indicated time at room temperature with 20 nM purified full-length recombinant human CaMKII α (#PV3142; Thermo Fisher Scientific), 2 μ M mCherry-Syn1, 0.03–2 μ M calmodulin or mCherry-CaM, 200 μ M CaCl₂ and 500 μ M ATP in a reaction buffer (50 mM Tris-HCl, pH 7.4, 10 mM MgCl₂, 2 mM DTT). The reactions were stopped at 10 min by adding SDS sample buffer and then analyzed by Western blotting. The following antibodies were used: Phospho-(Ser/Thr) PKA Substrate Antibody (#9621; Cell Signaling Technology) for phosphorylated mCherry-Syn1 detection; Goat Anti-Rabbit IgG (H + L)-HRP Conjugate (#1706515; Bio-Rad). We repeated the experiment four times from one preparation of the samples. Original images of the blots are in Source Data.

Plasmid construction for CaMKII α -CaM association imaging. We inserted cDNA sequence of calcium/calmodulin-dependent protein kinase II alpha (*Camk2a*) from *Rattus norvegicus* into the C-terminus of mEGFP containing pCAG plasmid, and calmodulin 1 (*calm1*) from *Mus musculus* into the C-terminus of mCherry containing pCAG plasmid. Molecular cloning and mutations were carried out using QuikChange site-directed mutagenesis kit (Agilent Technologies) and InFusion cloning kit (Clontech) for mEGFP-CaMKII α ^{T286A}, mEGFP-CaMKII α ^{T305A/T306A}, mEGFP-CaMKII α ^{T305D/T306D}, mEGFP-CaMKII α ^{T286A/305D/T306D}. The amount of transfected plasmids in the specified experiments are as follows: 1) mEGFP-CaMKII α ^{WT}/or mEGFP-CaMKII α ^{T286A} (20 μ g), and mCherry-CaM (40 μ g); 2) mEGFP-CaMKII α ^{T305D/T306D} or mEGFP-CaMKII α ^{T305A/T306A} (20 μ g), mCherry-CaM (40 μ g), and pCAG-Cre recombinase (12 μ g).

Microscope. The fluorescent lifetime of mEGFP-CaMKII α was measured by a home-built two-photon fluorescence lifetime imaging microscopy (2pFLIM). mEGFP-CaMKII α was excited with a Ti:Sapphire laser tuned at 920 nm (Coherent, Chameleon) with laser power measured under the water immersion objective (Olympus, NA = 1.0, \times 60) in the range of 1–1.5 mW^{19,38}. A second Ti:Sapphire laser at 720 nm (laser power measured under the objective: 2.5–3 mW), pulse duration of 4–6 ms was used to photolysis MNI-caged L-glutamate⁵.

CaMKII α -CaM association imaging. Hippocampal slices were bathed in artificial cerebrospinal fluid (ACSF) bubbled with carbogen (95% O₂/5% CO₂) during the image recordings. Final ion concentrations (in mM) in imaging solution: NaCl 127, NaHCO₃ 25, D-glucose 25, KCl 2.5, NaH₂PO₄ 1.25, supplemented with CaCl₂ 4, MNI-caged L-glutamate (Tocris) 4, TTX 0.001, Trolox (Sigma) 1. Between DIV 12–19, we imaged individual transfected CA1 pyramidal neurons. Dendritic spines on the secondary and tertiary apical dendrites were used for imaging. Images were acquired by a home-built 2pFLIM microscope controlled by custom software (MatLab or C#). Experiments were performed at 25 \pm 0.5 °C or 34–35 °C as indicated. The temperature was controlled with a control syringe heater and an inline solution heater (TC344C, SW-10/6 and SH-27B, Warner Instruments). Recordings were performed with 32 \times 32 pixels (pixel size: 12.3 \pm 1.72 pixel/ μ m) at 128 ms/frame (7.8 Hz). When we found a large drift of the position of the sample or significant photo-bleaching, we stopped the experiment and excluded from further analyses.

2pFLIM data analysis. The fluorescence lifetime of mEGFP-CaMKII α is affected by the FRET efficiency. The change of mean fluorescence lifetime of mEGFP-CaMKII α (τ_m) reflects the change of FRET efficiency and thus the binding fraction change of mEGFP-CaMKII α to mCherry-CaM. To measure the fraction of mEGFP-CaMKII α (donor) bound to mCherry-CaM (acceptor), the mean fluorescence lifetime of mEGFP-CaMKII α (τ_m) was derived from the mean photon arrival time t as follows:

$$\tau_m = t - t_0 = \frac{\int dt \cdot tF(t)}{\int dt \cdot F(t)} - t_0 \quad (1)$$

where $F(t)$ is the fluorescence lifetime decay curve, t_0 is offset. t_0 is estimated by fitting to the fluorescence decay curve summing all pixels in all frames over a whole image session (typically 1024 frames) with a double-exponential function convolved with the Gaussian pulse response function:

$$F(t) = F_0 [P_D H(t, t_0, \tau_D, \tau_G) + P_{AD} H(t, t_0, \tau_{AD}, \tau_G)] \quad (2)$$

where F_0 is constant, and

$$H(t, t_0, \tau_D, \tau_G) = \frac{1}{2} \exp\left(\frac{\tau_D^2}{2\tau_D} - \frac{t - t_0}{\tau_D}\right) \operatorname{erfc}\left(\frac{\tau_D^2 - \tau_D(t - t_0)}{\sqrt{2}\tau_D\tau_G}\right) \quad (3)$$

in which P_A and P_{AD} is the fraction of free donor and donor bound with acceptor, respectively, τ_D is the fluorescence lifetime of the donor without any bound acceptor ($\tau_D = 2.60$ ns), τ_{AD} is the fluorescence lifetime of the donor bound with acceptor ($\tau_{AD} = 1.09$ ns), τ_G is the width of the Gaussian pulse response function, F_0 is the peak fluorescence before convolution, t_0 is time offset, and erfc is the error function. τ_D and τ_{AD} are fixed during the curve fitting to obtain P_A and P_{AD} . For

regions of interests (ROI) within a field-of-view (such as spine and dendrite), the binding fraction P_{AD} is derived as follows:

$$P_{AD} = \frac{\tau_D(\tau_D - \tau_m)}{(\tau_D - \tau_{AD})(\tau_D + \tau_{AD} - \tau_m)} \quad (4)$$

Simulation of CaMKII α kinetics scheme. We constructed a set of rate equations (elementary reaction) to describe CaMKII α biochemical reactions based on the proposed CaMKII α kinetics model. The law of mass action was applied to obtain non-linear ordinary differential equations (ODEs) and to solve the concentration of each species. We implemented the algorithm written in Python. To simplify the simulation, the influx of NMDA-receptor mediated Ca^{2+} during repetitive glutamate uncaging is modeling as:

$$[Ca^{2+}] = A_i \exp(-[t - it_d]/\tau_{Ca}) + R \quad (t - id > 0) \quad (5)$$

where i is the number of uncaging pulses (integers, $i = 0 \dots 29, 30$ pulses), t_d is the uncaging interval (2 s), A_i is the peak $[Ca^{2+}]$ at i th uncaging pulse, $R = 50$ nM is the resting $[Ca^{2+}]$, and $\tau_{Ca} = 100$ ms is the Ca^{2+} decay time constant^{6,10,39}. Peak Ca^{2+} amplitude A_i decays after each uncaging pulse^{6,10,39}, perhaps due to desensitization of NMDARs⁴⁰. We model this as:

$$A_i = A_0(P_1 \exp[-i/\tau_n] + P_2), \quad (6)$$

where $A_0 = 4$ μ M is the peak $[Ca^{2+}]$ in response to the first uncaging pulse, and $\tau_n = 5$ is the decay constant, $P_1 = 0.5$ and $P_2 = 0.5$ are constants ($P_1 + P_2 = 1$).

For spike-timing-dependent plasticity (Fig. 7), we used:

$$[Ca^{2+}] = A \exp(-[t - it_d]/\tau_{Ca}) + R \quad (t - id > 0) \quad (7)$$

where $A = 0.8$ μ M and $\tau_{Ca} = 20$ ms for back-propagating action potentials (bAPs), and when paired with a synaptic release, $A = 2.4$ μ M was used. Because the synaptic release is simulated as a stochastic event, we repeated 20 times and averaged them for release probability < 1 .

Ca^{2+} binding to CaM was modeled using the previous scheme²². Thr286 phosphorylation occurs when two adjacent subunits are active⁹. We assume that the rate of phosphorylation of a subunit (k_1 , Fig. 6b) is proportional to the chance that the adjacent subunit is active:

$$k_1 = F k_{\text{phospho}}, \quad (8)$$

where $k_{\text{phospho}} = 12.6$ s^{-1} is the peak phosphorylation rate²³, and F is the active CaMKII fraction:

$$F = (KC_{CaM} + PC_{CaM} + P + P_2)/CaMKII_T, \quad (9)$$

where $CaMKII_T = 70$ μ M is the total CaMKII α subunit concentration^{6,22}. Total CaM concentration was assumed to be 30 μ M^{22,41}. Dephosphorylation before dissociation of CaM and rebinding of CaM to Thr286 phosphorylated-CaMKII α (P or P_2 , Fig. 6b and Fig. 7a) are assumed not to occur for the model in Fig. 6, following the previous models²². However, it is assumed to be 10% of the binding to non-phosphorylated CaMKII α in the model in Fig. 7. Kinetic parameters other than k_1 (k_2 – k_5) are obtained as follows: we obtain $k_2 = 1/3$ s^{-1} from the time constant of CaM dissociation (3 s) (Fig. 3c), and $k_3 = 1/6$ s^{-1} and $k_5 = 1/60$ s^{-1} from two time constants of CaMKII activity decay (6 s and 60 s)¹⁰. We obtain k_4 from the fraction of slow CaMKII decay (25%), which can be approximated by the ratio between k_3 and k_4 : $k_4 = 0.25 k_3$. The activity of autonomous activity was assumed to be 60% of that in the CaM bound form. All kinetic parameters are summarized in Table 1.

Statistical analysis. Error bars shown in the figures represent standard error of the mean (sem). sem of time constants is obtained by bootstrapping. The number of samples is indicated as the number of neurons/dendritic spines. Most of the slices have only one neuron.

Reporting summary. Further information on research design is available in the Nature Research Reporting Summary linked to this article.

Data availability

Time courses of all experiments and raw Western blot data are available in Data Source in Excel format. Original FLIM images will be available upon request.

Code availability

Python code for CaMKII α simulation is available on [GitHub](#). Matlab code for FLIM data acquisition and analysis is available on [GitHub](#). C# code for FLIM data acquisition and analysis is available on [GitHub](#).

Received: 14 November 2018 Accepted: 22 May 2019

Published online: 25 June 2019

References

- Rosenberg, O. S., Deindl, S., Sung, R. J., Nairn, A. C. & Kuriyan, J. Structure of the autoinhibited kinase domain of CaMKII and SAXS analysis of the holoenzyme. *Cell* **123**, 849–860 (2005).
- Elgersma, Y. et al. Inhibitory autophosphorylation of CaMKII controls PSD association, plasticity, and learning. *Neuron* **36**, 493–505 (2002).
- Silva, A. J., Paylor, R., Wehner, J. M. & Tonegawa, S. Impaired spatial learning in alpha-calcium-calmodulin kinase II mutant mice. *Science* **257**, 206–211 (1992).
- Silva, A. J., Stevens, C. F., Tonegawa, S. & Wang, Y. Deficient hippocampal long-term potentiation in alpha-calcium-calmodulin kinase II mutant mice. *Science* **257**, 201–206 (1992).
- Matsuzaki, M., Honkura, N., Ellis-Davies, G. C. & Kasai, H. Structural basis of long-term potentiation in single dendritic spines. *Nature* **429**, 761–766 (2004).
- Lee, S. J., Escobedo-Lozoya, Y., Szatmari, E. M. & Yasuda, R. Activation of CaMKII in single dendritic spines during long-term potentiation. *Nature* **458**, 299–304 (2009).
- Meyer, T., Hanson, P. I., Stryer, L. & Schulman, H. Calmodulin trapping by calcium-calmodulin-dependent protein kinase. *Science* **256**, 1199–1202 (1992).
- Miller, S. G. & Kennedy, M. B. Regulation of brain type II Ca^{2+} /calmodulin-dependent protein kinase by autophosphorylation: a Ca^{2+} -triggered molecular switch. *Cell* **44**, 861–870 (1986).
- Hanson, P. I., Meyer, T., Stryer, L. & Schulman, H. Dual role of calmodulin in autophosphorylation of multifunctional CaM kinase may underlie decoding of calcium signals. *Neuron* **12**, 943–956 (1994).
- Chang, J. Y. et al. CaMKII autophosphorylation is necessary for optimal integration of Ca^{2+} signals during LTP induction, but not maintenance. *Neuron* **94**, 800–808 e804 (2017).
- Giese, K. P., Fedorov, N. B., Filipkowski, R. K. & Silva, A. J. Autophosphorylation at Thr286 of the alpha calcium-calmodulin kinase II in LTP and learning. *Science* **279**, 870–873 (1998).
- Singla, S. I., Hudmon, A., Goldberg, J. M., Smith, J. L. & Schulman, H. Molecular characterization of calmodulin trapping by calcium/calmodulin-dependent protein kinase II. *J. Biol. Chem.* **276**, 29353–29360 (2001).
- Hanson, P. I., Kapiloff, M. S., Lou, L. L., Rosenfeld, M. G. & Schulman, H. Expression of a multifunctional Ca^{2+} /calmodulin-dependent protein kinase and mutational analysis of its autoregulation. *Neuron* **3**, 59–70 (1989).
- Lisman, J., Yasuda, R. & Raghavachari, S. Mechanisms of CaMKII action in long-term potentiation. *Nat. Rev. Neurosci.* **13**, 169–182 (2012).
- Colbran, R. J. Inactivation of Ca^{2+} /calmodulin-dependent protein kinase II by basal autophosphorylation. *J. Biol. Chem.* **268**, 7163–7170 (1993).
- Hashimoto, Y., Schworer, C. M., Colbran, R. J. & Soderling, T. R. Autophosphorylation of Ca^{2+} /calmodulin-dependent protein kinase II. Effects on total and Ca^{2+} -independent activities and kinetic parameters. *J. Biol. Chem.* **262**, 8051–8055 (1987).
- Takao, K. et al. Visualization of synaptic Ca^{2+} /calmodulin-dependent protein kinase II activity in living neurons. *J. Neurosci.* **25**, 3107–3112 (2005).
- Noguchi, J., Matsuzaki, M., Ellis-Davies, G. C. & Kasai, H. Spine-neck geometry determines NMDA receptor-dependent Ca^{2+} signaling in dendrites. *Neuron* **46**, 609–622 (2005).
- Yasuda, R. et al. Supersensitive Ras activation in dendrites and spines revealed by two-photon fluorescence lifetime imaging. *Nat. Neurosci.* **9**, 283–291 (2006).
- Pi, H. J., Otmakhov, N., Lemelin, D., De Koninck, P. & Lisman, J. Autonomous CaMKII can promote either long-term potentiation or long-term depression, depending on the state of T305/T306 phosphorylation. *J. Neurosci.* **30**, 8704–8709 (2010).
- Colbran, R. J. & Soderling, T. R. Calcium/calmodulin-independent autophosphorylation sites of calcium/calmodulin-dependent protein kinase II. Studies on the effect of phosphorylation of threonine 305/306 and serine 314 on calmodulin binding using synthetic peptides. *J. Biol. Chem.* **265**, 11213–11219 (1990).
- Pepke, S., Kinzer-Ursem, T., Mihalas, S. & Kennedy, M. B. A dynamic model of interactions of Ca^{2+} , calmodulin, and catalytic subunits of Ca^{2+} /calmodulin-dependent protein kinase II. *PLoS Comput Biol.* **6**, e1000675 (2010).
- Lucic, V., Greif, G. J. & Kennedy, M. B. Detailed state model of CaMKII activation and autophosphorylation. *Eur. Biophys. J.* **38**, 83–98 (2008).
- Otmakhov, N., Regmi, S. & Lisman, J. E. Fast decay of CaMKII FRET sensor signal in spines after LTP induction is not due to its dephosphorylation. *PLoS ONE* **10**, e0130457 (2015).

25. Coultrap, S. J., Buard, I., Kulbe, J. R., Dell'Acqua, M. L. & Bayer, K. U. CaMKII autonomy is substrate-dependent and further stimulated by Ca²⁺/calmodulin. *J. Biol. Chem.* **285**, 17930–17937 (2010).
26. Dan, Y. & Poo, M. M. Spike timing-dependent plasticity of neural circuits. *Neuron* **44**, 23–30 (2004).
27. Sabatini, B. L., Oertner, T. G. & Svoboda, K. The life cycle of Ca²⁺ ions in dendritic spines. *Neuron* **33**, 439–452 (2002).
28. Yasuda, R. et al. Imaging calcium concentration dynamics in small neuronal compartments. *Sci. STKE* **2004**, pl5 (2004).
29. Koester, H. J. & Sakmann, B. Calcium dynamics in single spines during coincident pre- and postsynaptic activity depend on relative timing of back-propagating action potentials and subthreshold excitatory postsynaptic potentials. *Proc. Natl Acad. Sci. USA* **95**, 9596–9601 (1998).
30. Strack, S., Barban, M. A., Wadzinski, B. E. & Colbran, R. J. Differential inactivation of postsynaptic density-associated and soluble Ca²⁺/calmodulin-dependent protein kinase II by protein phosphatases 1 and 2A. *J. Neurochem.* **68**, 2119–2128 (1997).
31. Colbran, R. J. Protein phosphatases and calcium/calmodulin-dependent protein kinase II-dependent synaptic plasticity. *J. Neurosci.* **24**, 8404–8409 (2004).
32. Zhabotinsky, A. M., Camp, R. N., Epstein, I. R. & Lisman, J. E. Role of the neurogranin concentrated in spines in the induction of long-term potentiation. *J. Neurosci.* **26**, 7337–7347 (2006).
33. Chao, L. H. et al. Intersubunit capture of regulatory segments is a component of cooperative CaMKII activation. *Nat. Struct. Mol. Biol.* **17**, 264–272 (2010).
34. Chao, L. H. et al. A mechanism for tunable autoinhibition in the structure of a human Ca²⁺/calmodulin-dependent kinase II holoenzyme. *Cell* **146**, 732–745 (2011).
35. Myers, J. B. et al. The CaMKII holoenzyme structure in activation-competent conformations. *Nat. Commun.* **8**, 15742 (2017).
36. Stoppini, L., Buchs, P. A. & Muller, D. A simple method for organotypic cultures of nervous tissue. *J. Neurosci. Methods* **37**, 173–182 (1991).
37. Murakoshi, H. et al. Kinetics of endogenous CaMKII required for synaptic plasticity revealed by optogenetic kinase inhibitor. *Neuron* **94**, 37–47 e35 (2017).
38. Murakoshi, H., Lee, S. J. & Yasuda, R. Highly sensitive and quantitative FRET-FLIM imaging in single dendritic spines using improved non-radiative YFP. *Brain Cell Biol.* **36**, 31–42 (2008).
39. Evans, P. R. et al. RGS14 restricts plasticity in hippocampal CA2 by limiting postsynaptic calcium signaling. *eNeuro* **5** ENEURO.0353-17.2018 (2018). <https://doi.org/10.1523/ENEURO.0353-17.2018>.
40. Sobczyk, A. & Svoboda, K. Activity-dependent plasticity of the NMDA-receptor fractional Ca²⁺ current. *Neuron* **53**, 17–24 (2007).
41. Kakiuchi, S. et al. Quantitative determinations of calmodulin in the supernatant and particulate fractions of mammalian tissues. *J. Biochem.* **92**, 1041–1048 (1982).

Acknowledgements

We thank Dr. Giese for *Camk2a*^{T286A} mice. We thank Dr. Murakoshi for His-tagged mCherry-Syn1. We thank members of the Yasuda lab for discussion, and Dr. Colgan and Dr. Raghavachari for the critical reading of the manuscript. We also thank M. Hu and J. Richards for preparing cultured slices and D. Kloetzer for laboratory management. This study was funded by Japan Society for the Promotion of Science (YN), NIH (R01MH111486, R01MH080047, and 1DP1NS096787), and the Brain Research Foundation.

Author contributions

J.Y.C. and R.Y. designed the experiments. J.Y.C. performed most of the imaging experiments, Y.H. performed biochemical experiments, and Y.N. performed fluorescence lifetime measurements in HeLa cells. J.Y.C. and R.Y. constructed the simulation, analyzed the data and wrote the paper. All authors discussed the results and commented on the manuscript.

Additional information

Supplementary Information accompanies this paper at <https://doi.org/10.1038/s41467-019-10694-z>.

Competing interests: R.Y. is a founder of Florida Lifetime Imaging LLC, a company that helps people set up FLIM. The remaining authors declare no competing interests.

Reprints and permission information is available online at <http://npg.nature.com/reprintsandpermissions/>

Peer review information: *Nature Communications* thanks Peter Giese, and the other, anonymous, reviewer(s) for their contribution to the peer review of this work. Peer reviewer reports are available.

Publisher's note: Springer Nature remains neutral with regard to jurisdictional claims in published maps and institutional affiliations.



Open Access This article is licensed under a Creative Commons Attribution 4.0 International License, which permits use, sharing, adaptation, distribution and reproduction in any medium or format, as long as you give appropriate credit to the original author(s) and the source, provide a link to the Creative Commons license, and indicate if changes were made. The images or other third party material in this article are included in the article's Creative Commons license, unless indicated otherwise in a credit line to the material. If material is not included in the article's Creative Commons license and your intended use is not permitted by statutory regulation or exceeds the permitted use, you will need to obtain permission directly from the copyright holder. To view a copy of this license, visit <http://creativecommons.org/licenses/by/4.0/>.

© The Author(s) 2019